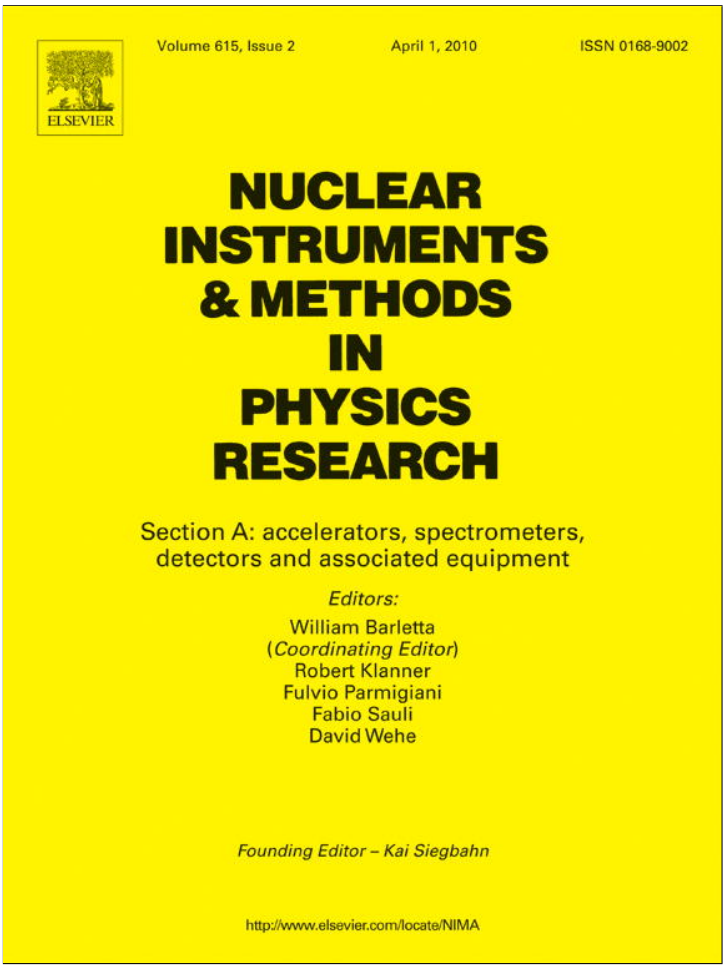

Nuclear Instruments and Methods in Physics Research A 615 (2010) 230–236

Contents lists available at ScienceDirect

Nuclear Instruments and Methods in Physics Research A

journal homepage: www.elsevier.com/locate/nima

Impact of plasma effects on the performance of silicon sensors at an X-ray FEL

Julian Becker *,[1], Doris Eckstein [1], Robert Klanner [1], Georg Steinbrück [1]

Institute for Experimental Physics, Detector Laboratory, University of Hamburg, Luruper Chaussee 149, 22761 Hamburg, Germany

ARTICLE INFO

Article history:
Received 8 December 2009
Received in revised form
27 January 2010
Accepted 30 January 2010
Available online 6 February 2010

Keywords:
Plasma effects
Silicon sensor
X-rays
XFEL
AGIPD
Charge explosion

ABSTRACT

The impact of electron hole plasmas on silicon sensor performance was studied with a multi-channel Transient Current Technique (mTCT) setup. Electron hole densities of up to $10^{16}\,cm^{-3}$ (equivalent to 10^5 focused 12 keV photons) were created with sub-ns lasers (660 and 1015 nm) and the time resolved current pulses of segmented sensors (4 channels simultaneously) were read out by a 2.5 GHz oscilloscope. Measurements for strip sensors of 280 μm thickness and 80 μm pitch as well as 450 μm thickness and 50 μm pitch were carried out showing an increase of the charge collection time and an increase of the charge spread (charge cloud explosion) with increased charge carrier density. These effects were studied as a function of the applied bias voltage and electron hole density. It was shown that for the current AGIPD sensor design plasma effects in p-in-n sensors of 450 μm thickness are negligible if at least 500 V bias is applied.

1. Introduction

The European XFEL [1] will push the limits of brilliance further than any light source today. The expected dynamic range, from single photons to 10^5 12 keV photons per pixel per pulse, is a challenge to the design of silicon sensors and front end electronics [2–5].

At the European XFEL the photon energy will be tunable from 12.4 to 0.8 keV. The XFEL pulses will be of short duration (<100 fs) and have a bunch repetition rate of 5 MHz (200 ns spacing). A super-cycle of 3000 bunches is followed by 99.4 ms idle time (10 Hz) [6].

The high number of photons per pixel per pulse will create charge carrier densities exceeding the bulk doping of the sensor which will influence among others the linearity, point spread function and response time of the detector.

The main physical effect of these so-called electron hole plasmas is the change of the electric field inside the sensor. In the low density case this change is small and can be neglected, whereas in the case of high densities the changed electric field plays a dominant role in the charge collection process.

Due to self-shielding effects inside the plasma ambipolar diffusion becomes the dominant transport process, changing the induced current pulse of the sensor and increasing the charge collection time by a so-called plasma time [7]. Plasma effects have shown to decrease as the electric field increases [8]. Using incident ions of varying mass and energy, the influence of sensor properties on plasma effects has been studied in detail in Ref. [9].

However, the plasma effects observed for heavy ions are not expected to be observed at the European XFEL, as the created charge carrier densities will be orders of magnitude lower than those created by high-Z ions.

The plasma effects change the charge collection process. Carriers will drift apart laterally due to two processes: diffusion and electrostatic repulsion. At first diffusion is the dominant process as electrons and holes are not separated. Once the charges are separated mutual electrostatic repulsion, which increases with charge carrier density, increases the lateral spread.

These two effects will result in an increased lateral spread of the collected charge and thus in increased charge sharing between pixels, as shown recently in Ref. [10] for α−particles. It was shown in Ref. [11] that this spread is a strong function of the electric field inside the sensor and thus of the bias voltage. High bias voltages reduce the self-shielding effects of high charge carrier densities.

All measurements in this work have been performed using light with perpendicular incidence. Results for oblique incidence are expected to show less plasma effects and asymmetric charge spreading as shown in Ref. [12] for light ions.

* Corresponding author. Tel.: +49 40 8998 4725; fax: +49 40 8998 2959.
E-mail address: Julian.Becker@desy.de (J. Becker).
[1] On behalf of the AGIPD Consortium (http://hasylab.desy.de/science/developments/detectors/agipd/agipd_members/index_eng.html).

0168-9002/$ - see front matter © 2010 Elsevier B.V. All rights reserved.
doi:10.1016/j.nima.2010.01.082

2. Experimental setup

To study the impact of the electron hole plasma a multi-channel Transient Current Technique (mTCT) setup was built. Charge carrier densities up to $10^{16}\,cm^{-3}$ (corresponding to 10^5 12 keV photons in a small spot) were created with sub-ns lasers (660 and 1015 nm) and the time resolved current pulses of the investigated sensors (4 channels simultaneously) were read out by Miteq AM-1309 wideband amplifiers and a Tektronix DPO 7254 2.5 GHz oscilloscope. The transfer function of the whole setup has been checked and was found to introduce distortions on the sub-ns level, which were considered insignificant.

The samples were mounted on a special substrate that allowed light injection from both sides while cooling them to 20 °C and simultaneously providing the high voltage to the rear side of the sensor.

The sample holder and optics were mounted on translation stages controlling the position of light injection with 0.1 μm accuracy.

2.1. Laser properties

The laser system was manufactured by Picoquant GmbH [13] and provided short and intense laser pulses with a FWHM <100 ps. The system uses exchangeable laser heads, each head providing light of different wavelength. For this study laser light with an average wavelength of 660 nm (± 2 nm) and 1015 nm (± 6 nm) was used. The maximum pulse energy is 140 and 260 pJ for the 660 and 1015 nm laser, respectively.

In silicon the number of optical and X-ray photons decreases exponentially with thickness. The attenuation length of 660 nm light and 1 keV photons is 3 μm. One thousand and fifteen nm light and 12 keV photons have an attenuation length of roughly 250 μm (calculated from the mass energy absorption coefficient of 12 keV photons).

It should be noted that is a statistical process involving secondary process like Compton scattering and fluorescence. Thus the energy transferred to the silicon lattice (and therefore the initial electron hole distribution) can only be described by an exponential function with an infinite number of impinging photons. However, the statistical fluctuations of deposited energy per unit path length become negligible when a few hundred photons are absorbed simultaneously. So lasers can only be used to simulate the energy distribution of many X-ray photons, not the absorption of individual X-ray photons.

The laser beam was focused to a spot with Gaussian profile with $\sigma \leq 3$ μm. In air the Rayleigh length (distance from focal point to the point where the beam radius increases by $\sqrt{2}$) is approximately 90 μm. This guarantees a focused laser beam for 1015 nm light through the entire thickness of the silicon sensors used in this work, as the high refractive index of silicon effectively increases the Rayleigh length inside the silicon by a factor of approximately 3.6. Different pulse energies have been created by using optical attenuation, which has no influence of the spot size and pulse duration.

2.2. Investigated sensors

Two microstrip sensors have been investigated. The overall size (substrate) of the microstrip sensors was 10 mm $\times$ 10 mm, the strip length about 8 mm. Both sensors are p-in-n sensors (structured p+ implant (front) in n-type silicon (bulk), continuous n+ implant(rear)).

The sensor of 280 μm thickness, which has a strip pitch of 80 μm and a p + implantation width of 20 μm, was produced by CiS Forschungsinstitut für Mikrosensorik und Photovoltaik GmbH [14]. The silicon used is high resistivity n-type diffusion oxygenated float zone silicon with ⟨1 0 0⟩ orientation manufactured by Wacker. The effective doping, determined from a diode test structure on the wafer is $8 \times 10^{11}\,cm^{-3}$. The depletion voltage for the 280 μm strip sensor is 63 V.

The sensor of 450 μm thickness, which has a strip pitch of 50 μm and a p + implantation width of 11 μm, was produced by Hamamatsu Photonics [15]. The silicon used is high resistivity n-type silicon with ⟨1 1 1⟩ orientation. The depletion voltage for the 450 μm strip sensor is 155 V.

The 280 μm sensor has an aluminum grid on the back contact that allows laser light injection opposite to the strips. The aluminum on the rear contact of the 450 μm sensor was removed to allow light injection from the rear side.

The readout electronics was on ground potential. To ensure proper working conditions five strips on both sides of the readout strips were also connected to ground potential. The bias voltage was applied to the rear side.

3. Results

All results presented were obtained with rear side illumination.

The generated charge is given as equivalent photons by dividing the number of electron hole pairs by the number of electron hole pairs created by a photon of 1 keV (278 e,h pairs) or 12 keV energy (3333 e,h pairs).

There is a difference in the number of absorbed and incident 12 keV photons, as the conversion probability of a 12 keV photon in 280 and 450 μm of silicon is roughly 0.73 and 0.88, respectively.

3.1. Increase of charge collection time

From the measured transients the charge collection time is determined as a function of bias voltage and charge carrier density. A few selected transients for 660 and 1015 nm light are shown in Figs. 1 and 3.

Without plasma effects the charge collection times range from 6 to 20 ns (500 and 100 V, respectively) for the 280 μm sensor and from 12 to 30 ns (500 and 200 V, respectively) for the 450 μm sensor.

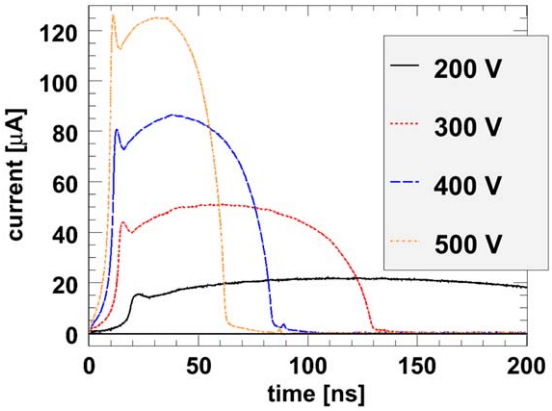

Fig. 1. Transients obtained for the 450 μm sensor. Focused 660 nm light of high intensity (≈ 3 μm rms, 3.24×10^5 1 keV photons) was injected from the rear side, centered to the readout strip. Transients are presented for different applied bias voltages, showing an almost rectangular shape, plasma delays and very long charge collection times for low voltages. The depletion voltage of this sensor is 155 V.

Please cite this article as: J. Becker, et al., Nucl. Instr. and Meth. A (2010), doi:10.1016/j.nima.2010.01.082

Fig. 1 shows recorded transients (pulse shapes) of the 450 μm sensor. Focused 660 nm light of high intensity (≈ 3 μm rms, 3.24 $\times 10^5$ 1 keV photons) was injected from the rear side, centered to the readout strip. Plasma delays (i.e. time needed to reach a certain threshold) are clearly visible and decreasing for increased voltage. The charge collection process is extremely prolonged and the current pulses exhibit a local peak around the undisturbed charge collection time. The charge collection time is observed to be strongly dependent on the applied voltage.

Charge collection times as a function of applied voltage and charge carrier density are shown in Fig. 2. For high densities and low voltages the charge collection time exceeds 200 ns, which is the bunch repetition time of the European XFEL. Thus it is important to carefully match the bias voltage and integration time of the preamplifier in the readout electronics to avoid nonlinearities.

Fig. 3 shows the effect of different spot sizes. A larger spot size reduces the charge carrier density and therefore the associated increase in charge collection time due to plasma effects.

Fig. 4 shows the cumulative current pulse ($Q(t)$-diagram) as a function of the applied voltage for the equivalent of injecting 1.63 $\times 10^5$ focused 12 keV photons. It can be seen that at 500 V bias voltage all the charge is collected in roughly 60 ns.

Memory (or pile-up) effects appear when less than 100% of the charge is collected during the bunch repetition time. This can be avoided when more than 300 V bias voltage are applied (shown in Fig. 4).

3.2. Charge cloud explosion

The strip geometry allows sensitive measurements, and by evaluating the recorded transients the spatial distribution of the charge cloud can be reconstructed. Position and voltage scans were performed as a function of intensity to study the influence of the charge carrier density. The transients were integrated to yield the collected charge, and the collected charge versus position plot (collected charge profile) was used to evaluate the point spread function for this density by a fitting procedure. The point spread function was parameterized as a convolution of a semi-circle and a Gaussian distribution. For the fitting procedure the following equations were used:

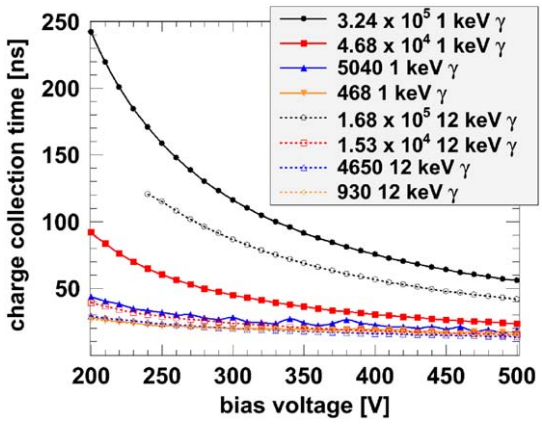

Fig. 2. Charge collection time obtained for the 450 μm sensor as a function of the applied bias voltage for different intensities. Focused light (≈ 3 μm rms) was injected from the rear side, centered to the readout strip. The charge collection time was determined as the time between injection and the point where 95% of the total charge was collected (for transients see Fig. 1). Charge collection times as low as 60 ns are reached for the highest intensity (3.24 $\times 10^5$ 1 keV photons) when 500 V bias is applied. The depletion voltage of the sensor is 155 V.

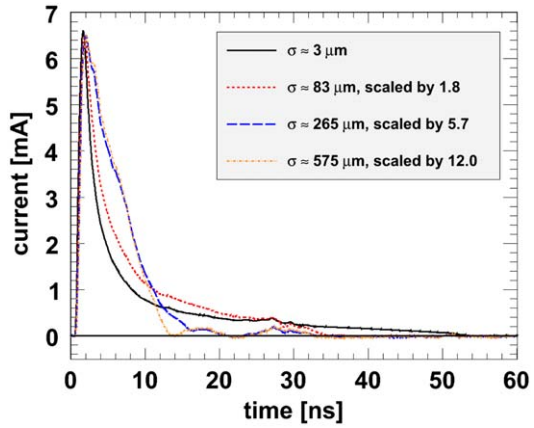

Fig. 3. Transients obtained for the 450 μm sensor. 1015 nm light of high intensity ($\approx 1.5 \times 10^5$ 12 keV photons) was injected from the rear side, centered to the readout strip. Transients are presented for 500 V applied bias voltage and different spot sizes, showing the dependence of the pulse shape on photon density. The integrated charge measured on the readout strip decreases as the injected charge distributes over more and more strips, thus the curves have been renormalized to the most focused one. A small distortion is observed between t = 26 and 32 ns due to impedance mismatches in the readout circuit.

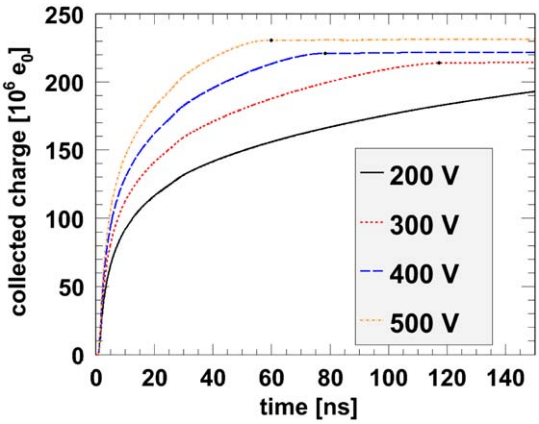

Fig. 4. Integrated transients (charge pulse) obtained for the 450 μm sensor. Focused 1015 nm light of high intensity (≈ 3 μm rms, 1.68 $\times 10^5$ absorbed 12 keV photons) was injected from the rear side, centered to the readout strip. Charge pulses are presented as a function of time for different applied bias voltages. The charge collected on the strip increases with voltage as the size of the charge cloud decreases.

$$Q(x_{inj}) = N_p \int_{\mu-p/2}^{\mu+p/2} PSF(\hat{x}-x_{inj})d\hat{x} + R(x_{inj}) \quad (1)$$

$$PSF(x) = (f \otimes g)(x) \quad (2)$$

$$f(x) = \frac{1}{\sigma_p\sqrt{2\pi}} \exp\left(-\frac{x^2}{2\sigma_p^2}\right) \quad (3)$$

$$g(x) = \frac{2}{\pi r^2}\sqrt{r^2-x^2} \quad (4)$$

where Q is the charge collected on the strip, N_p the number of electron hole pairs created by the primary light, μ the strip center position, p the strip pitch, x_{inj} the center of the laser light distribution, σ_p and r the parameters of the PSF and $R(x_{inj})$ a reflection term. The reflection term is needed for 1015 nm light in contrast to 660 nm light ($R(x_{inj}) = 0\ \forall x_{inj}$) as not all light is absorbed within the bulk material. Some light reaches the front side and is reflected back into the bulk at the strip metalization.

Please cite this article as: J. Becker, et al., Nucl. Instr. and Meth. A (2010), doi:10.1016/j.nima.2010.01.082

This additional light leads to an apparent "boost" in the collected charge signal (see Fig. 6).

Additionally the reflected light has its own distribution, which is different from the distribution of the primary light. This distribution was modeled by summing the contributions of readout, neighbor and next neighbor strips, as a signal boost was also observed when hitting the metalization of the neighbor and next neighbor strip. The reflection term was parameterized the following way:

$$R(x) = \sum_{i=-2}^{2} \frac{N_{|i|}}{\sigma_l \sqrt{2\pi}} \int_{x-w/2}^{x+w/2} \exp\left(-\frac{(\hat{x}-\mu+ip)^2}{2\sigma_l^2}\right) d\hat{x} \quad (5)$$

where $N_{|i|}$ the number of electron hole pairs created by reflected light, which is usually two orders of magnitude lower than the number of electron hole pairs created by primary light and $N_0 \geq N_1 \geq N_2 \geq 0$, w the metal width on top of the p+ implantation and σ_l the standard deviation of the injected laser light. The reflection term (5) is zero for 660 nm light, as no light reaches the strip metalization ($N_0 = N_1 = N_2 = 0$).

The collected charge as a function of position of injection and corresponding fits are shown in Figs. 5 and 6. The chosen parameterization gives a good description of the data.

The collected charge profiles have been fitted with Eq. (1) and radius and sigma of the point spread function were extracted as a function of bias voltage and laser intensity. Using the extracted parameters the point spread function (PSF) was reconstructed. The reconstructed PSFs of the 450 μm sensor for different applied bias voltages for 660 and 1015 nm light of different intensities are shown in Figs. 7 and 9, respectively. It is observed that at 500 V applied bias the PSF for up to 10^4 12 keV photons and up to 10^5 1 keV photons stays well confined within the foreseen pixel size of the AGIPD sensor (200 μm).

All PSFs measured for the 280 μm sensor and the 450 μm sensor are available in tabulated form in the online version of this article (Figs. 7 and 9).

From the tabulated data of the PSFs the modulation transfer functions (MTFs) and autocorrelation functions (ACFs) have been calculated for 200 and 500 V bias voltage. MTFs and ACFs are shown in Figs. 8 and 10 for injection of 660 and 1015 nm light, respectively. The MTF is defined as the magnitude of the Fourier transform of the PSF and, as the PSF is available as discrete real

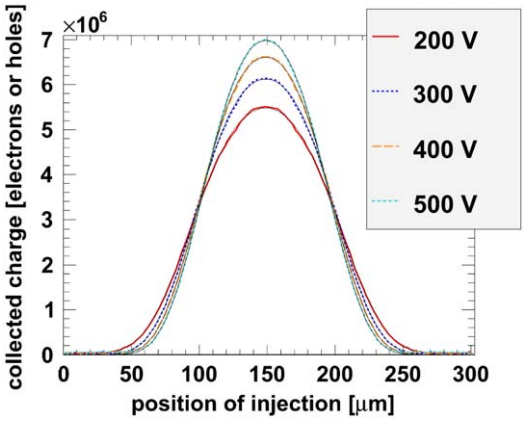

Fig. 5. Charge collected on one strip of the 450 μm sensor as a function of injection location, obtained from position scans with 2 μm step size. Focused 660 nm light (3 μm rms) was used to inject an equivalent of 4.68 × 10^4 1 keV photons. The thin black lines show the fit to the measurement data. The maximum of the curve does not reproduce the number of created electron hole pairs, as the created charge is distributed over several strips (charge sharing).

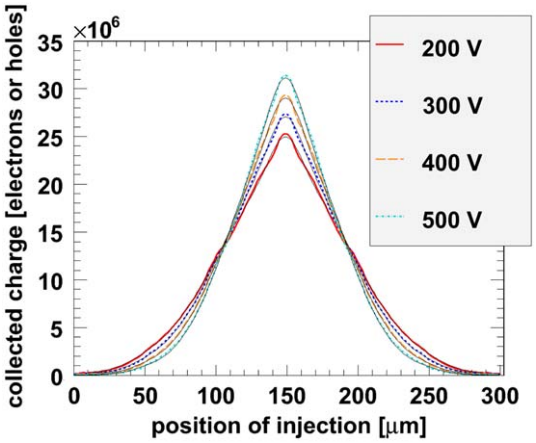

Fig. 6. Charge collected on one strip of the 450 μm sensor as a function of injection location, obtained from position scans 2 μm step size. Focused 1015 nm light (3 μm rms) was used to inject an equivalent of 1.53 × 10^4 12 keV photons. The thin black lines show the fit to the measurement data. The maximum of the curve does not reproduce the number of created electron hole pairs, as the created charge is distributed over several strips (charge sharing). The increase of collected charge due to light reflections at the strip metalization is visible at $x \approx 100$ μm, $x \approx 150$ μm and $x \approx 200$ μm.

values, the ACF was calculated using the following equation:

$$ACF(x_i) = \sum_n PSF(x_n) \times PSF(x_{n-i}). \quad (6)$$

Points of special interest on the MTF are the point where the MTF drops to 0.5, which marks up to which spatial frequency images can be resolved, and the value at the inverse pixel size (0.005 μm^{-1}). At the inverse pixel size the MTF is above 0.5 in all cases; however, distinguishing image points with a difference in brightness requires a higher contrast (value of the MTF). It is observed that the contrast at a fixed spatial frequency decreases strongly when the charge carrier density is increased. An increase of contrast is observed when the applied voltage is increased; however, this effect is small compared to the effect of the increased charge carrier density.

4. Discussion and conclusions

A multi-channel TCT system was set up with the following properties: short (<100 ps FWHM) and intense (up to 250 pJ) laser pulses, focused to create electron hole plasmas. A 2.5 GHz bandwidth oscilloscope was used for readout.

The laser spot was very small compared to the expected size of Bragg peaks in XFEL experiments. This means the results presented for tight focusing are to be seen as a worst case estimate.

Charge collection times have been measured and it was shown that at 500 V bias voltage the charge collection times are about 60 ns, which does not exceed the integration time of the charge sensitive preamplifier of the AGIPD detector.

Using strip sensors, the shape of the point spread function has been measured for different electron hole densities and operating voltages. It was found that the data can be described by the convolution of a Gaussian distribution with a semi-circle.

It has been shown that at 500 V applied bias the PSF for up to 10^4 12 keV photons and up to 10^5 1 keV photons stays well confined within the foreseen pixel size of the AGIPD sensor (MTFs >0.5 at the inverse pixel size).

Plasma effects manifest in both the time and spatial domain. It has been shown that at a fixed bias voltage the charge collection

Please cite this article as: J. Becker, et al., Nucl. Instr. and Meth. A (2010), doi:10.1016/j.nima.2010.01.082

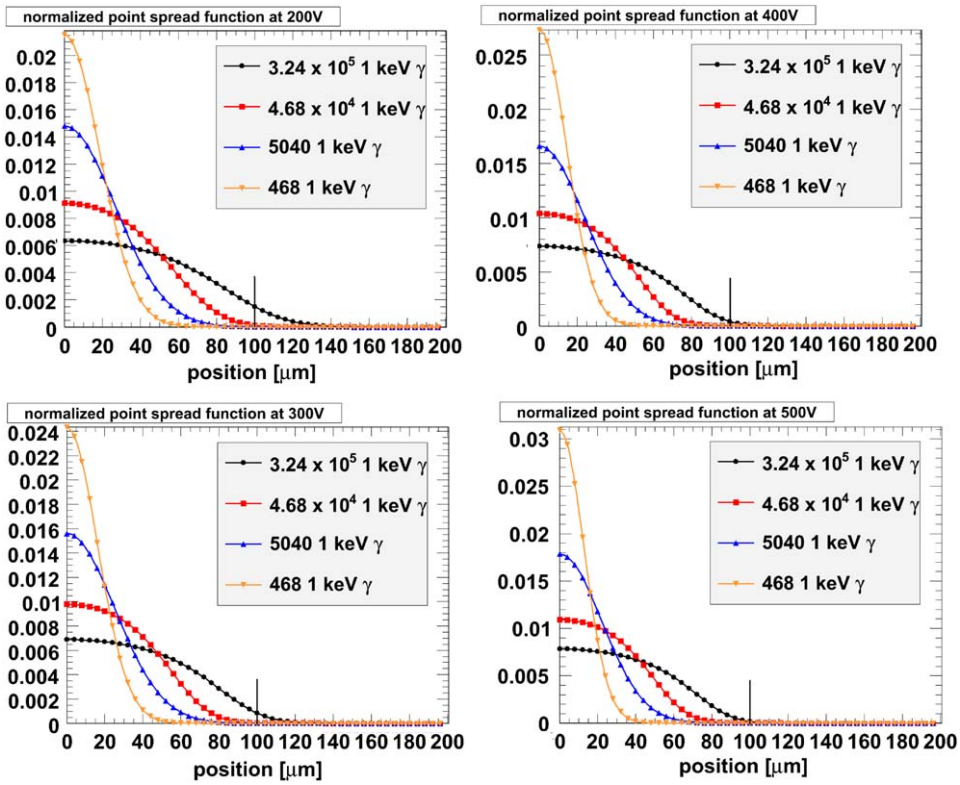

Fig. 7. Reconstructed point spread function of the 450 μm sensor for 200, 300, 400 and 500 V bias voltage for 660 nm light of different intensities. The sigma of the injected light is ≈3 μm. The PSF is symmetric along the *x*-axis. The vertical line at 100 μm position indicates the AGIPD pixel size for comparison. At 500 V all PSFs stay confined within the pixel size.

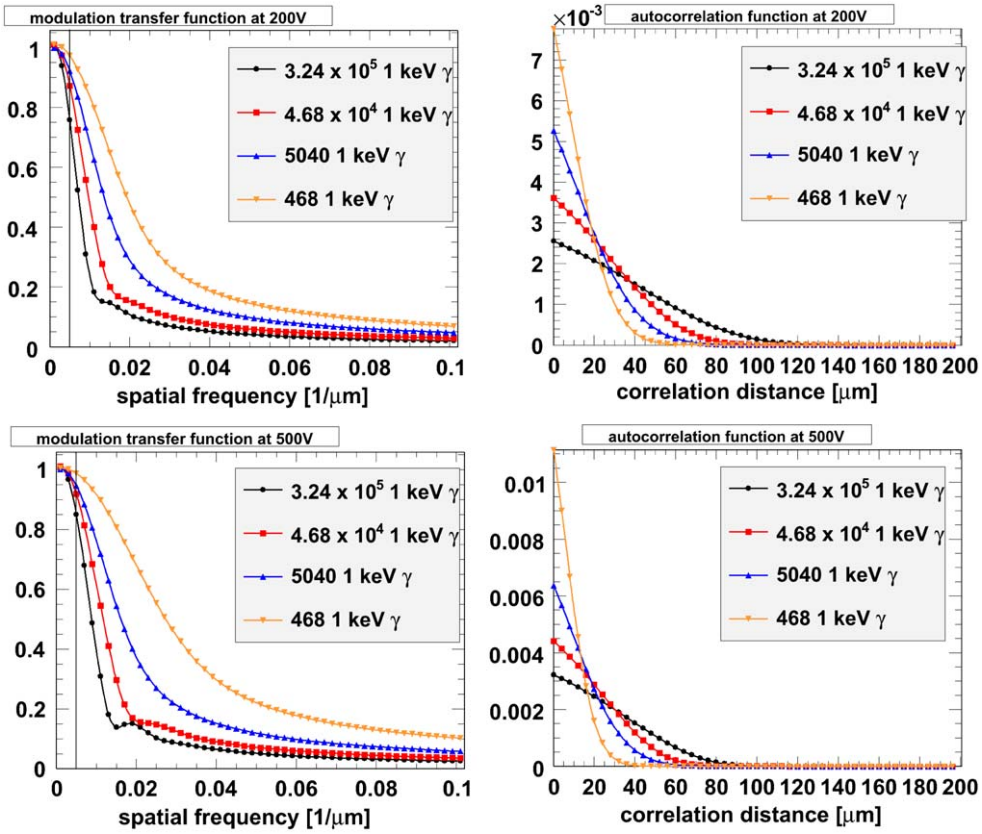

Fig. 8. Modulation transfer function and autocorrelation function of the 450 μm sensor for 200 and 500 V bias voltage for 660 nm light of different intensities. The sigma of the injected light is ≈3 μm. The vertical line at 0.005 μm^{-1} spatial frequency indicates the inverse AGIPD pixel size for comparison. All MTFs are above 0.5 at the inverse pixel size. Both MTFs and ACFs are a strong function of the charge carrier density and weakly dependent on bias voltage.

Please cite this article as: J. Becker, et al., Nucl. Instr. and Meth. A (2010), doi:10.1016/j.nima.2010.01.082

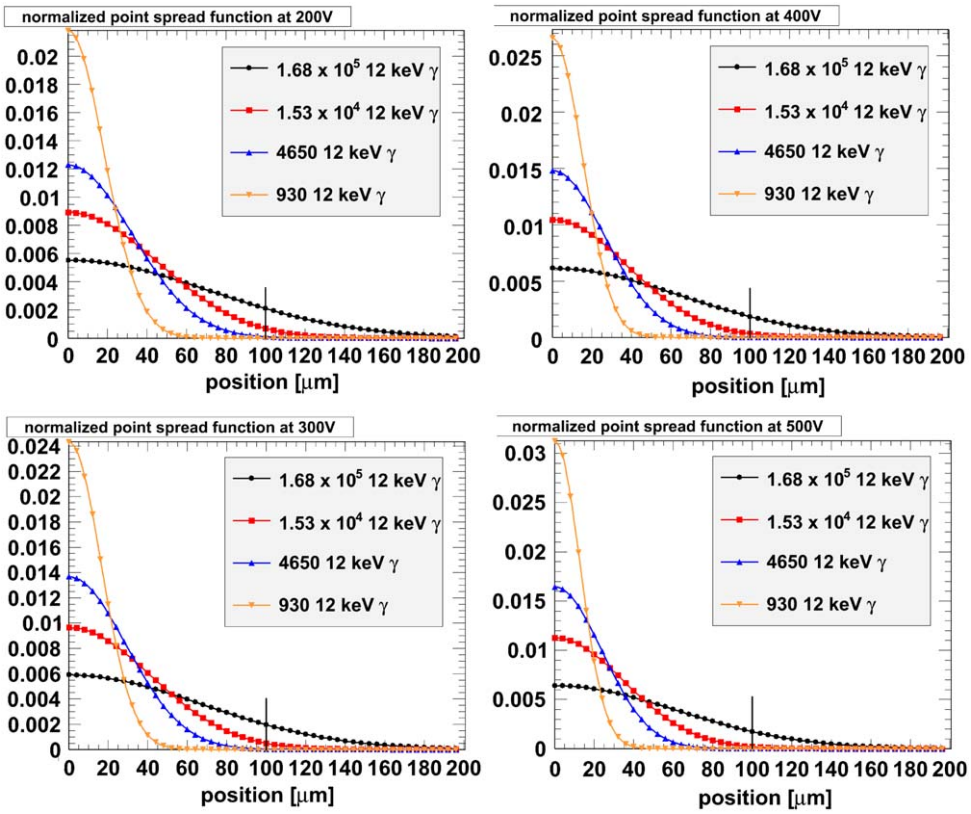

Fig. 9. Reconstructed point spread function of the 450 μm sensor for 200, 300, 400 and 500 V bias voltage for 1015 nm light of different intensities. The sigma of the injected light is ≈3 μm. The PSF is symmetric along the *x*-axis. The vertical line at 100 μm position indicates the AGIPD pixel size for comparison. At 500 V all PSFs except for 1.68 $\times 10^5$ 12 keV photons stay confined within the pixel size.

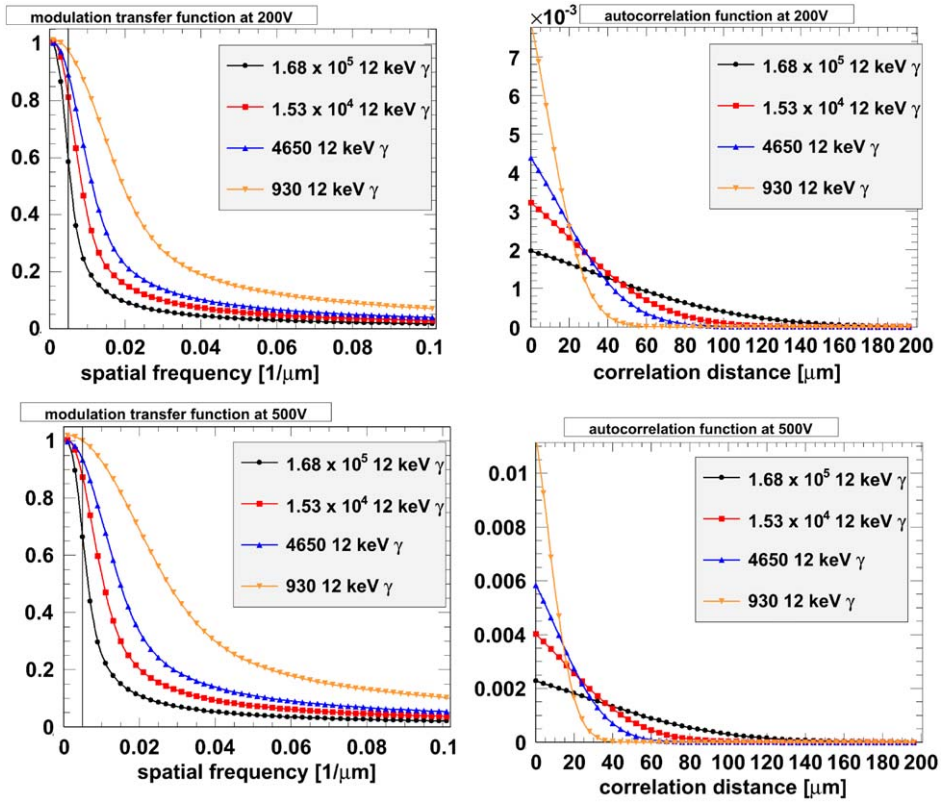

Fig. 10. Modulation transfer function and autocorrelation function of the 450 μm sensor for 200 and 500 V bias voltage for 1015 nm light of different intensities. The sigma of the injected light is ≈3 μm. The vertical line at 0.005 μm^{-1} spatial frequency indicates the inverse AGIPD pixel size for comparison. All MTFs are above 0.5 at the inverse pixel size. Both MTFs and ACFs are a strong function of the charge carrier density and weakly dependent on bias voltage.

Please cite this article as: J. Becker, et al., Nucl. Instr. and Meth. A (2010), doi:10.1016/j.nima.2010.01.082

time and the pixel size has to be increased in order tolerate plasma effects in the imaging process.

Acknowledgments

We would like to thank Dr. E. Fretwurst for providing the samples of 280 μm thickness and insightful discussions.

This work was partly funded by the Helmholtz Alliance "Physics at the Terascale", the Federal Ministry of Education and Research and the European XFEL Consortium.

References

[1] The European XFEL ⟨http://www.xfel.eu/en/index.php⟩.
[2] The AGIPD detector ⟨http://hasylab.desy.de/science/developments/detectors/agipd/index_eng.html⟩.
[3] AGIPD (former HPAD) reply to the Call for Expression of Interest available at ⟨http://xfel.desy.de/project_group/work_packages/photon_beam_systems/wp_75_detector_development/2d_x_ray_detectors/eoi_replies/⟩.
[4] G. Potdevin, et al., Nucl. Instr. and Meth. A 607 (2009) 51.
[5] B. Henrich, et al., in: Proceedings of the 11th iWoRiD Conference, Prague, Czech Republic, June 28–July 2, 2009, Nucl. Instr. and Meth. A, to be published.
[6] Technical Design Report of the European XFEL available at ⟨http://xfel.desy.de/tdr/tdr/⟩.
[7] W. Seibt, K.E. Sundström, P.A. Tove, Nucl. Instr. and Meth. 113 (1973) 317.
[8] R.N. Williams, E.M. Lawson, Nucl. Instr. and Meth. 120 (1974) 261.
[9] W. Bohne, W. Galster, K. Grabisch, H. Morgenstern, Nucl. Instr. and Meth. A 240 (1985) 145.
[10] M. Campbell, et al., Nucl. Instr. and Meth. A 591 (2008) 38.
[11] J. Becker, D. Eckstein, R. Klanner, G. Steinbrück, in: Proceedings of the 11th European Symposium on Semiconductor Detectors, Wildbad Kreuth, Germany, June 7–11, 2009, Nucl. Instr. and Meth. A, to be published.
[12] J. Bouchami, et al., Nucl. Instr. and Meth. A 607 (2009) 196.
[13] PicoQuant GmbH website ⟨http://www.picoquant.de/⟩.
[14] CiS Forschungsinstitut für Mikrosensorik und Photovoltaik GmbH website ⟨http://www.cismst.de/⟩.
[15] Hamatsu Photonics ⟨http://www.hamamatsu.com/⟩.

Please cite this article as: J. Becker, et al., Nucl. Instr. and Meth. A (2010), doi:10.1016/j.nima.2010.01.082